Solvothermal Synthesis of Three-Dimensional Hierarchical CuS Microspheres from a Cu-Based Ionic Liquid Precursor for High-Performance Asymmetric Supercapacitors

Jing Zhang,[†,‡] Huijie Feng,[†,‡] Jiaqin Yang,[†,‡] Qing Qin,[†,‡] Hongmin Fan,[†,‡] Caiying Wei,[†,‡] and Wenjun Zheng*,[†,‡]

[†]Key Laboratory of Advanced Energy Materials Chemistry (MOE), TKL of Metal and Molecule-based Material Chemistry, College of Chemistry, and [‡]Collaborative Innovation Center of Chemical Science and Engineering, Nankai University, Tianjin, 300071, China

S Supporting Information

ABSTRACT: It is meaningful to exploit copper sulfide materials with desired structure as well as potential application due to their cheapness and low toxicity. A low-temperature and facile solvothermal method for preparing three-dimensional (3D) hierarchical covellite (CuS) microspheres from an ionic liquid precursor $[Bmim]_2Cu_2Cl_6$ (Bmim = 1-butyl-3-methylimidazolium) is reported. The formation of CuS nanostructures was achieved by decomposition of intermediate complex $Cu(Tu)_3Cl$ (thiourea = Tu), which produced CuS microspheres with diameters of 2.5−4 μm assembled by nanosheets with thicknesses of 10−15 nm. The ionic liquid, as an "all-in-one" medium, played a key role for the fabrication and self-assembly of CuS nanosheets. The alkylimidazolium rings ($[Bmim]^+$) were found to adsorb onto the (001) facets of CuS crystals, which inhibited the crystal growth along the [001] direction, while the alkyl chain had influence on the assembly of CuS nanosheets. The CuS microspheres showed enhanced electrochemical performance and high stability for the application in supercapacitors due to intriguing structural design and large specific surface area. When this well-defined CuS electrode was assembled into an asymmetric supercapacitor (ASC) with an activated carbon (AC) electrode, the CuS//AC-ASC demonstrated good cycle performance (~88% capacitance after 4000 cycles) and high energy density (15.06 W h kg^{-1} at a power density of 392.9 W kg^{-1}). This work provides new insights into the use of copper sulfide electrode materials for asymmetric supercapacitors and other electrochemical devices.

KEYWORDS: copper sulfide, ionic liquid, nanostructures, three-dimensional, asymmetric supercapacitor, energy storage, conversion
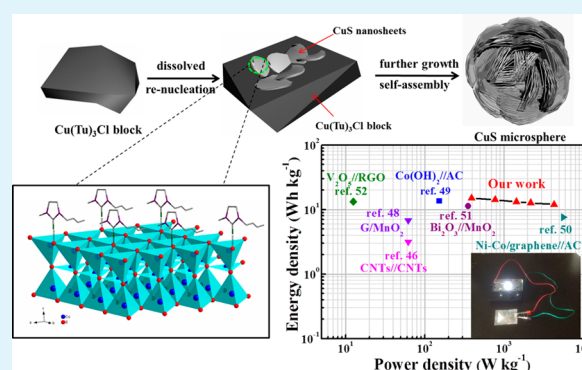
INTRODUCTION

As a bottom-up approach, self-assembly of low-dimensional (e.g., one-dimensional (1D) nanorods, two-dimensional (2D) nanosheets) building blocks into their higher-order three-dimensional (3D) multifunctional superstructures is a fascinating technique to achieve a wide range of novel functional materials with regular architectures.[1] The architectures and properties of inorganic materials are believed to show a close relationship. Three-dimensional hierarchical micro/nanostructures have a distinct ability for electron transfer and stability of the structure compared with 1D and 2D nanostructures, which integrate the advantages of the nanoscale building blocks and their assembled architectures.[2,3] As an important p-type semiconductor, copper sulfide (CuS) is a kind of cheap and environmentally friendly semiconductor due to its abundance and low toxicity.[4] Thus, CuS is a promising option for applications in photothermal conversion, biosensors, gas sensors, Li ion batteries, catalysts, superionic materials, and solar cell devices.[5−7] Rencently, CuS has been found to show potential application as a supercapacitor.[8−10] However, low areal capacitances, slow rate capabilities, and low energy densities of CuS electrodes are still big challenges. One of the solutions to these problems lies in controlling the structure of CuS materials. Extensive studies have focused on the synthesis of CuS 3D hierarchical architectures by various controllable synthetic strategies to promote their application properties. These structures include wool-ball-like micro-flowers,[11] hierarchical ball-flowers,[12] shuttlelike bundles,[13] concave polyhedral superstructures,[14] nanostructures assembled of nanoplates, nanoparticles, and nanotubes,[15] complex symmetrical nanostructures,[16] hierarchical hexagonal stacked plates,[17] and so on. However, few reports pay close attention to improving the supercapacitor performance of CuS electrodes through the designed 3D hierarchical architectures. Furthermore, these methods either involve mostly surfactant- or template-assisted pathways or require high temperature,

which increases the reaction complexity as well as the energy consumption. Therefore, it remains a big challenge to exploit a simple and environmentally friendly strategy to synthesize CuS materials with devisable 3D hierarchical architectures for application in supercapacitors.

Recently, ionic liquids (ILs) have been considered as a new type of green alternative solvents owing to their unique physical and chemical properties.[18] As a definition of supramolecular fluids, ILs can construct expanded hydrogen-bond systems in the liquid state and display an outstanding ability to self-assemble different nanostructures due to the existence of large number of noncovalent interactions (such as van der Waals forces, electrostatic interactions, hydrogen bonding, and $\pi-\pi$ stacking).[19] In particular, ionic liquid (IL) precursor can serve as an "all-in-one" solvent to simplify the reaction system and then control the structures and compositions of the final products.[20] Until now, many nanomaterials, such as BiOX (X = Cl, Br, I), ferric giniite, Ag/AgCl composites, CuSe nanoflakes, iron-based fluoride nanomaterials, and α-Fe_2O_3 cubes, were successfully synthesized by the "all-in-one" ILs.[21−27] In the formation of the above nanostructures, the final devisable architectures were achieved by the surface adsorption and orientation arrangement of ILs.

Due to the numerous advantages of ILs, we look forward to employing ILs for the synthesis of CuS with expected 3D hierarchical structure. Up to now, there have been several studies on the preparation of CuS by using ILs. For example, CuS nestlike hollow spheres[28] could be prepared via an oil−water interface method from the IL 1-butyl-3-methylimidazolium tetrafluoroborate ([Bmim]BF_4). However, the obtained CuS microstructures were nonuniform, with large quantities of CuS microcrystallites concomitantly generated. Then Yao et al.[29] obtained uniform flowerlike CuS nanostructures by the IL [C_8mim][BF_4], but a toxic solvent, $CHCl_3$, was used in the reaction. In this paper, we introduced an IL precursor [Bmim]$_2Cu_2Cl_6$ as a Cu source, and developed a solvothermal method to fabricate well-defined 3D CuS hierarchical structures. The major benefits of the present route are lower temperature, simpler reaction system, and greater security compared to the previous studies. The as-prepared hierarchical CuS microspheres were assembled by thin CuS sheets. The IL acted as solvent−reactant−template, which not only guided the growth direction, but also conducted the assembly of CuS nanosheets. As expected, the CuS electrode shows high capacitance values, great rate capability, and good cycling ability. Furthermore, an asymmetric supercapacitor (ASC) assembled by CuS microspheres and activated carbon (AC) as positive and negative electrodes reveals a high energy density of 15.06 W h kg^{-1} at a power density of 392.9 W kg^{-1}, indicating the potential application of CuS as a long-term performance electrode material for asymmetric supercapacitor device.

■ EXPERIMENTAL DETAILS

Materials. All reagents were of analytical grade and were used without further purification. Ionic liquids [$C_x$mim]Cl (x = 4, 8; 1-butyl-3-methylimidazolium chloride and 1-octyl-3-methylimidazolium chloride) were purchased from Shanghai Chengjie Chemical Co. Ltd.

Synthesis of [Bmim]$_2Cu_2Cl_6$. For the synthesis of [Bmim]$_2Cu_2Cl_6$, 0.01 mol of [Bmim]Cl and 0.01 mol of $CuCl_2$ were mixed and added into a three-necked flask with stirring. The mixture was heated by oil bath at 85 °C for 12 h, and then the product [Bmim]$_2Cu_2Cl_6$ was collected and dried at 80 °C under vacuum for 6 h. [Bmim]$_2CuCl_4$ was synthesized by 0.03 mol of [Bmim]Cl and 0.01 mol of $CuCl_2$, and [Omim]$_2Cu_2Cl_6$ was synthesized by 0.01 mol of

[Omim]Cl and 0.01 mol of $CuCl_2$, keeping the other experimental conditions unchanged. The general structural feature of [Bmim]$_2Cu_2Cl_6$ is shown in Figure S1.

Synthesis of 3D Hierarchical CuS Microspheres. In a typical synthesis, 0.31 g of [Bmim]$_2Cu_2Cl_6$ (0.5 mmol) was added into 24 mL of absolute ethanol under stirring to form a homogeneous green solution. Then, 0.304 g of thiourea (4 mmol) was added under continuous stirring; the color of the solution was changed from green to white. After stirring for 10 min, the mixture was transferred into a 30 mL Teflon-lined autoclave, sealed, and heated at 100 °C for 20 h. After being cooled to room temperature, the resulted solid was centrifuged and washed with deionized water and anhydrous ethanol three times. The as-prepared samples were dried at 60 °C for 12 h. For comparison, CuS samples were also prepared by using [Bmim]$_2CuCl_4$, [Omim]$_2Cu_2Cl_6$, and $CuCl_2·2H_2O$ as precursors with the same Cu amount under the same conditions.

Characterization. The products were characterized by XRD, SEM, EDS, XPS, TEM, high-resolution (HR) TEM, and BET measurements. Powder X-ray diffraction (XRD) measurements were conducted on a Rigaku-Dmax 2500 diffractometer with Cu Kα radiation (λ = 0.1518 nm). Scanning electron microscopy (SEM) images were carried out on a JEOL JSM-6700F field emission scanning electron microscope (15 kV) coupled with energy dispersive X-ray spectroscopy (EDS). The chemical states of the elements were determined on Kratos Axis Ultra DLD multitechnique X-ray photoelectron spectrometer (XPS). Transmission electron microscopy (TEM) images were performed with a Tecnai G2 F20 TEM. The nitrogen adsorption−desorption isotherm was determined using the Brunauer−Emmett−Teller (BET) equation by a surface area analyzer ASAP 2020 (Micromeritics).

Electrochemical Measurements. Electrochemical activities of the as-prepared 3D hierarchical CuS microspheres were evaluated by a three-electrode arrangement in 2 M KOH electrolyte. An Hg/HgO electrode and bright Pt plate were used as the reference electrode and counter electrode, respectively. The working electrodes were fabricated by mixing the active material (3D hierarchical CuS microspheres or platelike CuS prepared by $CuCl_2·2H_2O$), acetylene black, and polyvinylidene fluoride (PVDF) in N-methyl-2-pyrrolidone (NMP) with a weight ratio of 8:1:1. In our experiment, about 2.4 mg of active materials was loaded on a piece of nickel foam (1.0 cm × 1.0 cm); the actual mass is determined by weighing. A Zahner IM6e electrochemical workstation was used for conducting cyclic voltammetry (CV) analyses with voltage scan rates of 5, 10, 20, 50, and 100 mV s^{-1}. A LAND battery system was used for galvanostatic charge−discharge (CD) investigations at the current densities of 0.5, 1, 2, 3, 5, and 8 A g^{-1}. The specific capacitance is calculated according to the following equation:

$$C = \frac{I\Delta t}{m\Delta V} \qquad (1)$$

where C (F g^{-1}) represents the specific capacitance, I (A) designates the discharge current, Δt (s) is the total discharge time, m (g) is the mass of active materials, and ΔV (V) is the potential drop during discharge.

Fabrication of the Asymmetric Supercapacitor. For the fabrication of the asymmetric supercapacitor, CuS microspheres and AC were used as the positive and negative electrodes, respectively. The separator was cellulose paper, and the electrolyte was 2 M KOH. The voltammetric charges (Q) can be evaluated as follow:

$$Q = C \Delta V m \qquad (2)$$

where C represents the specific capacitance (F g^{-1}) of each electrode, ΔV is the potential window (V) of each electrode, and m is the mass loading (g) of each electrode. To achieve a charge balance of the ASC, the voltammetric charges of the positive electrode and the negative electrode followed the equation $Q_+ = Q_-$. Therefore, the mass ratio of the positive electrode and negative electrode followed the equation

$$\frac{m_+}{m_-} = \frac{C_- \Delta V_-}{C_+ \Delta V_+} \tag{3}$$

In our experiment, the specific capacitance values of AC and CuS electrodes are 115 and 204 F g^{-1} at a current density of 2 A g^{-1}. According to the potential windows of the two electrodes, the mass ratio is calculated to be $m_+/m_- = 1.13$ in CuS//AC-ASC.

The energy density E (W h kg^{-1}) and power density P (W kg^{-1}) were calculated as follows:

$$E = \frac{C \Delta V^2}{2} \frac{1000}{3600} \tag{4}$$

$$P = \frac{E}{\Delta t} \cdot 3600 \tag{5}$$

where C represents the specific capacitance (F g^{-1}) and ΔV designates the potential range (V); Δt is the discharge time (s).

■ RESULTS AND DISCUSSION

CuS 3D hierarchical architectures are prepared by the reaction of an ethanol solution of [Bmim]$_2$Cu$_2$Cl$_6$ (the general structural feature is shown in Figure S1) with thiourea at 100 °C for 20 h. The XRD pattern of the product is shown in Figure 1a. All of the diffraction peaks can be well indexed to the
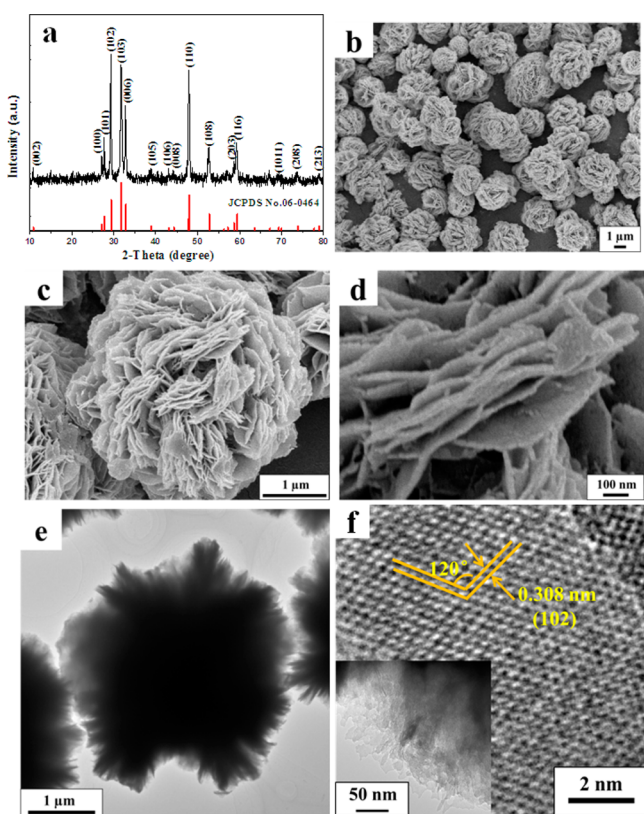

Figure 1. (a) XRD pattern, (b−d) SEM images, (e) TEM image, and (f) HRTEM image of as-prepared 3D hierarchical CuS microspheres. The inset of (f) is a TEM image of nanosheets that built up the CuS microstructures.

hexagonal phase of CuS (covellite type, space group $P6_3/mmc$), with the lattice parameters of $a = 3.792$ Å and $c = 16.344$ Å (JCPDS No. 06-0464). No other peaks of impurities indicate the high purity of the sample. Compared with the standard XRD pattern for CuS, the (102) reflection peak is remarkably

enhanced, which reveals that the CuS crystals are growth-oriented.[30]

The morphological feature of the as-prepared CuS microspheres was observed by SEM and TEM images, as shown in Figure 1b−f. The low magnification (Figure 1b) of the 3D CuS architectures indicates that the as-prepared products are large-scale microspheres with diameters of 2.5−4 μm. The high-magnification SEM images (Figure 1c,d) reveal that the entire 3D hierarchical CuS structures are formed by interdigitation of bunches of nanosheets, and the average thickness of CuS nanosheets is ca. 10 nm. The EDS pattern (Figure S2) of the product clearly revealed that the obtained product only consisted of Cu and S elements. The atomic ratio of Cu to S is found to be approximately 1:1, confirming the stoichiometry of CuS. Figure 1e shows a panoramic TEM image of a single spherelike microstructure; the microspheres are assembled by CuS nanosheets, which validates the SEM results. The inset of Figure 1f indicates that these nanosheets are composed of several ultrathin subnanosheets. As can be seen from the HRTEM image (Figure 1f), two apparent lattice fringes reveal both the interplanar distance at ca. 0.308 nm and the intersection angle of approximately 120° indicating the (102) plane sets of the CuS microstructures, which corresponds to the XRD result. Because of the intrinsic anisotropic characteristic of CuS layered nanostructure, the CuS crystals are possibly preferentially oriented along the [102] direction, and restrained along the [001] direction.[7,17,30]

Time-dependent experiments were carried out to investigate the evolution process of CuS 3D hierarchical microspheres. The results of XRD profiles and SEM images are shown in Figure 2 and 3, respectively. With maintaining the temperature
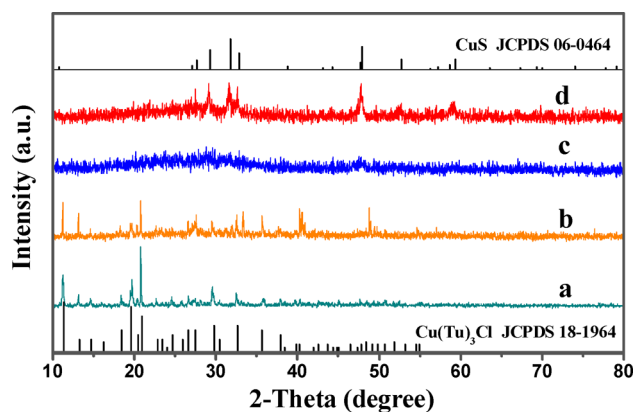
Figure 2. XRD patterns of as-obtained products after different reaction times: (a) 6, (b) 12, (c) 14, and (d) 15 h. Tu = CS(NH$_2$)$_2$.

at 100 °C for 6 h, the product was pure-phase intermediate complex Cu(Tu)$_3$Cl blocks (Figures 2a and 3a). When the reaction continued for 12 h, CuS was found to coexist with Cu(Tu)$_3$Cl (Figure 2b); it could be seen that some CuS nanosheets existed on the surface of Cu(Tu)$_3$Cl blocks (Figure 3b). On prolonging the reaction time to 14 h, the vast majority of Cu(Tu)$_3$Cl decomposed (Figure 3c). The distinct characteristic peaks of Cu(Tu)$_3$Cl were not found from the XRD pattern (Figure 2c); the low intensity of peaks may be due to the poor crystallinity of CuS nanosheets. EDS pattern and XPS analysis (Figure S3) show that the product only consisted of Cu and S elements; the atomic ratio of Cu to S is ca. 1:1, as shown in Table S1. The valences of Cu and S correspond to CuS
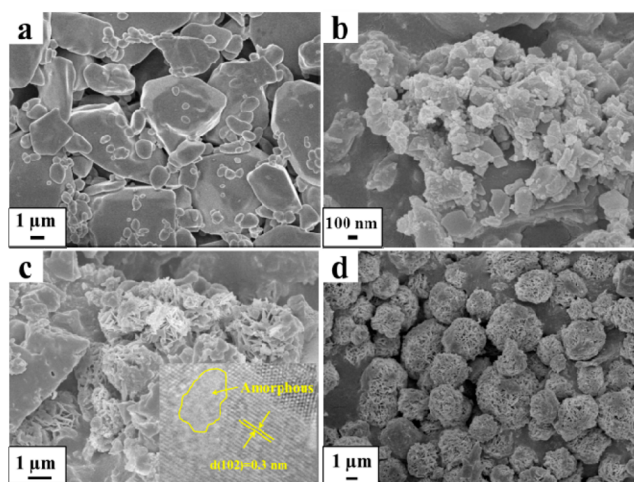
Figure 3. SEM images of as-obtained products after different reaction times: (a) 6, (b) 12, (c) 14, and (d) 15 h.

Scheme 1. Phase Transformation from Cu(Tu)₃Cl into CuS[a]

[a]Color code of the atoms: blue, Cu; red, S; gray, C; yellow, N; green, Cl. H atoms are omitted for clarity.

according to XPS.[31] The result indicates that $Cu(Tu)_3Cl$ decomposed completely. High-resolution TEM (inset of Figure 3c) shows the clear lattice fringes which further corroborate the formation of CuS nanostructure. However, some amorphous components indicate that the structure of CuS is not intact. With further increasing the reaction time to 15 h, the XRD pattern only showed pure CuS (Figure 2d), revealing a complete phase transition into CuS. The spherelike structure assembled by CuS nanosheets was formed as shown in Figure 3d.

According to the above results, it could be concluded that the formation of CuS can be divided into three stages: (i) the formation of intermediate complex $Cu(Tu)_3Cl$ blocks, (ii) their conversion into CuS nanosheets at low reaction rate, and (iii) assembly of CuS nanosheets into 3D microspheres. To reveal the phase transformation from $Cu(Tu)_3Cl$ into CuS, we investigated the crystal structure of intermediate complex $Cu(Tu)_3Cl$ and the final product CuS. As reported previously,[32,33] the crystal structure of $Cu(Tu)_3Cl$ is ionic, containing chloride ions and alternate −Cu−S−Cu−S−Cu−S− helical chains of cationic $[Cu(Tu)_3]^+$ (Figure S4a). In the polymeric chain, Cu^+ ions are tetrahedrally coordinated by four sulfur atoms from surrounding thiourea ligands, and two of thiourea ligands act as a bridge between Cu atoms. Interestingly, the structure of hexagonal CuS crystal (Figure S4b) consists of alternative two [CuS] tetrahedron layers and a [CuS] triangle plane layer in the c direction. The structural similarity between $Cu(Tu)_3Cl$ and CuS crystals ensured the successful transformation from $Cu(Tu)_3Cl$ to CuS; a postulate of the structure evolution process was put forward as shown in Scheme 1. Part of the tetrahedron chains connected with each other to form a [CuS] tetrahedron layer, while the rest first transformed to [CuS] triangle plane chains and then polymerized to a [CuS] triangle plane layer. Finally, two tetrahedron layers and one triangle plane layer built a new layered structure of CuS crystals. In this way, CuS nanosheets renucleate through the heterogeneous nucleation pathway accompanied by the dissolution of the $Cu(Tu)_3Cl$ blocks.
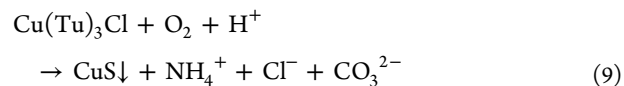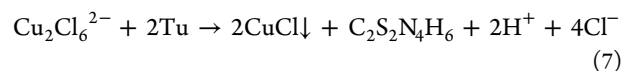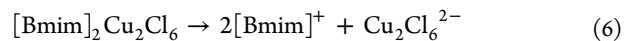
On the basis of the above analysis, the whole reaction process can be demonstrated. It could be conjectured that when $[Bmim]_2Cu_2Cl_6$ was dissolved in ethanol solution, $Cu_2Cl_6^{2-}$ was released from the IL. Then an amount of thiourea was added into the reaction system. Because of the interaction
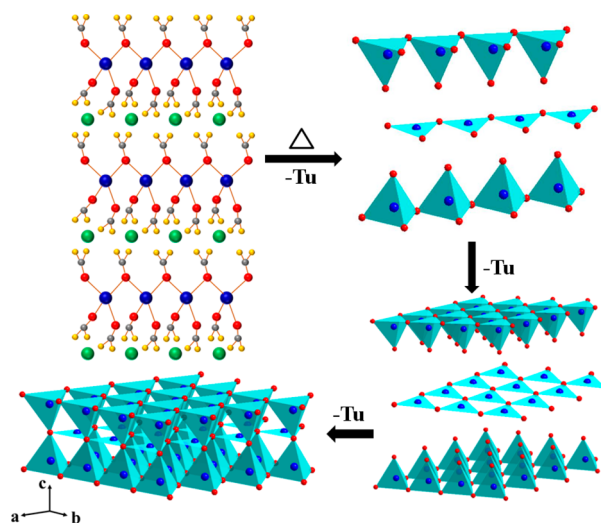
between Cl^- and the Lewis acidic H atoms in the C_2 position of $[Bmim]^+$ rings (Figure S1), thiourea molecular can easily attack Cu^{2+}, and thence CuCl precipitation was obtained by the rapid reaction between $Cu_2Cl_6^{2-}$ with thiourea. In this case, trace amounts of Cu^+ dissociated by CuCl would coordinate with Tu rather than Cl^- to form $Cu(Tu)_3^+$, because of the strong complexing ability between Cu^+ and Tu ($Cu(Tu)_3^+$, log β_3 = 13; $CuCl_2^-$, $CuCl_3^{2-}$, log β_2 = 5.5, log β_3 = 5.7).[34] Then $Cu(Tu)_3^+$ would rapidly react with Cl^-, which consequently caused CuCl precipitation gradually transformed into $Cu(Tu)_3Cl$ precipitation. The color of the solution tuned from green to brown, and finally to white, as seen in Figure S5. After being maintained at 100 °C for a long time, $Cu(Tu)_3Cl$ intermediate slowly decomposed into CuS. The corresponding reaction process can be expressed as in eqs 6−9. Note that the temperature and long reaction time are indispensable for the decomposition of $Cu(Tu)_3Cl$, which was conducive to the fabrication of CuS nanosheets and their assembly into CuS microspheres.

$$[Bmim]_2Cu_2Cl_6 \rightarrow 2[Bmim]^+ + Cu_2Cl_6^{2-} \tag{6}$$

$$Cu_2Cl_6^{2-} + 2Tu \rightarrow 2CuCl\downarrow + C_2S_2N_4H_6 + 2H^+ + 4Cl^- \tag{7}$$

$$CuCl + 3Tu \rightarrow Cu(Tu)_3Cl \tag{8}$$

$$Cu(Tu)_3Cl + O_2 + H^+$$
$$\rightarrow CuS\downarrow + NH_4^+ + Cl^- + CO_3^{2-} \tag{9}$$

To investigate the effect of $[Bmim]_2Cu_2Cl_6$ on the morphology of CuS, CuS samples were prepared by $CuCl_2·2H_2O$ and $[Bmim]_2CuCl_4$ instead of $[Bmim]_2Cu_2Cl_6$. As shown in Figure S6, when $CuCl_2·2H_2O$ is used as Cu source, the final products are a disordered platelike structure with a thickness of about 80 nm. However, when $[Bmim]_2CuCl_4$ is employed, the products maintain the spherelike structure assembled by nanosheets. Therefore, it can be seen that IL precursor serves a key role for guiding the fabrication of thin CuS nanosheets.

The effect of $[Bmim]_2Cu_2Cl_6$ on the formation of CuS sheetlike architectures may be explained from the view of crystal growth habit and dynamics. As can be seen from Figure S7, the interactions between a [CuS] tetrahedron layer and a [CuS] triangle layer are covalent bonds, while the interactions within the S—S layers are *van der Waals* interactions (the green bond in Figure S7). The intrinsic anisotropic characteristics cause the growth of CuS crystal along the top—bottom crystalline planes rather than along the c-axis.[35] When $Cu(Tu)_3Cl$ decomposed into CuS nucleus, $[Bmim]^+$ would adsorb on the surface of CuS nucleus due to the Lewis acidity of the H atoms in the C_2 position of $[Bmim]^+$ rings. $[Bmim]^+$ prefers to adsorb on the thermodynamically stable (001) plane to minimize the surface energy of the structure, which is similar to CuSe nanoflakes that are prepared in the presence of an IL precursor.[25]

Scheme 2a shows the atom arrangement of the covellite CuS crystal viewed from the [001] direction. Obviously, in various

Scheme 2. (a) Corresponding Crystallographic Model of CuS Covellite Structure Viewed from the [001] Direction;[a] (b) Shape Evolution from $Cu(Tu)_3Cl$ into CuS; (c) Schematic Illustration of a Projected View of $[Bmim]^+$ Ions Absorbed on the (001) Surface of CuS To Form a Layer
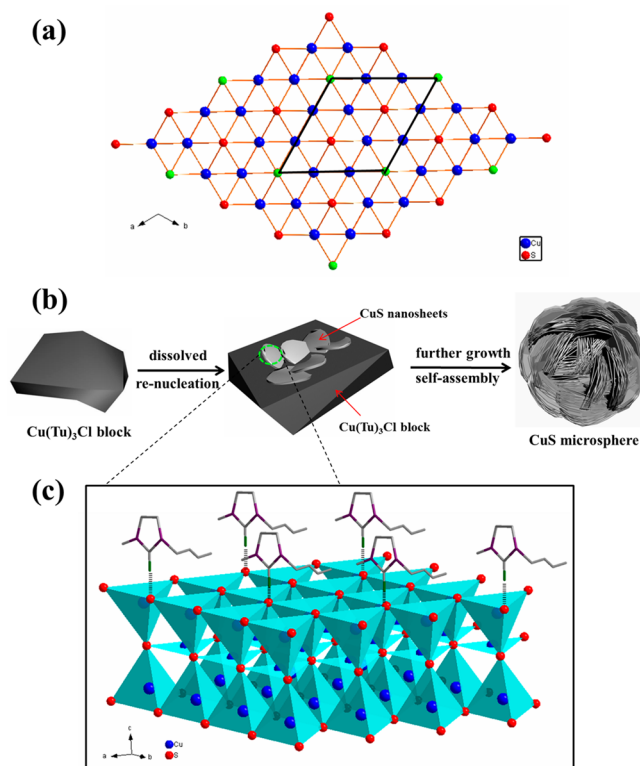

[a]The green balls indicate the S ions adsorbed with $[Bmim]^+$ ions.

directions, all the distances between adjacent S atom adsorption sites are 0.65 nm, which is suitable for the distance of the $\pi-\pi$ stack (0.6–0.7 nm) between the imidazole rings.[36] The result also conforms to the geometric matching principle, which is proved in our previous work about the adsorption of IL on the substrate.[37] Scheme 2b shows a schematic illustration of the effect of IL on the shape evolution from $Cu(Tu)_3Cl$ into CuS. When $Cu(Tu)_3Cl$ blocks dissolved into CuS nucleus, $[Bmim]^+$ ions would vertically adsorb on the (001) plane of CuS

crystal;[38] a relatively tight coverage layer on the CuS surface is formed through the π-stacking interactions (Scheme 2c). Thus, the growth of the CuS crystal along the [001] direction is restrained, thereby leading to the formation of CuS nanostructure that prevents the direction vertical to the (001) crystal plane. Finally, CuS crystal growth mainly processes oriented growth to form thin sheetlike CuS.

The other influence of ILs on the formation of CuS microstructures is that ILs contribute to the assembly of sheetlike CuS into 3D hierarchical architectures. In our work, $[Omim]_2Cu_2Cl_6$ was used as precursor to disclose the effect of alkyl chain length. An SEM image (Figure S8) shows that a spherelike structure assembled by nanosheets is obtained. However, the arrangement of the nanosheets is orderly, and the intervals among the nanosheets are even larger. It is indicated that long-chain IL tends to form a loose hierarchical structure. There may be two reasons for this: one is that IL tends to form thermotropic liquid crystal with the increasing of alkyl chain length,[39] and the arrangement of $[Bmim]^+$ ions is more orderly along a preferred direction; additionally, long-chain ILs possess large steric effects to form a tighter coverage layer, which effectively prevents the penetration of substances. Overall, by means of surface adsorption and self-assembly, IL is able to successfully control the morphology of CuS. The as-obtained CuS 3D hierarchical structure composed of thin nanosheets will provide the possibility of high specific surface area and efficient electron transfer.

The nitrogen adsorption and desorption isotherms of CuS thin nanosheet 3D structures (marked as S-1) and thick platelike structures (synthesized by $CuCl_2 \cdot 2H_2O$, marked as S-2) are shown in Figure 4. Both materials exhibited a typical IV
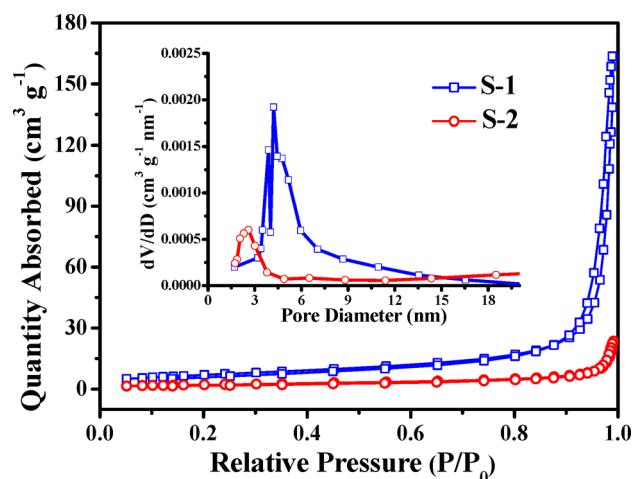
Figure 4. N_2 adsorption−desorption isotherms with corresponding pore size distribution plots (inset) of S-1 and S-2.

isotherm, which indicated mesoporous features of the two materials. The BET specific surface area of the CuS microspheres (S-1) was 25.6 $m^2 g^{-1}$, which is 3.3 times larger than that of CuS nanoplates (S-2, 7.8 $m^2 g^{-1}$). The average pore diameters of both materials were placed in the mesopore region (inset of Figure 4): the maxima were centered at 4.2 and 2.3 nm for S-1 and S-2, respectively. The high BET specific surface area and well-developed mesoporous structure of CuS microspheres are advantageous for energy storage applications due to their capability to promote electrolyte penetration and ion transport, and provide more active sites for electrochemical
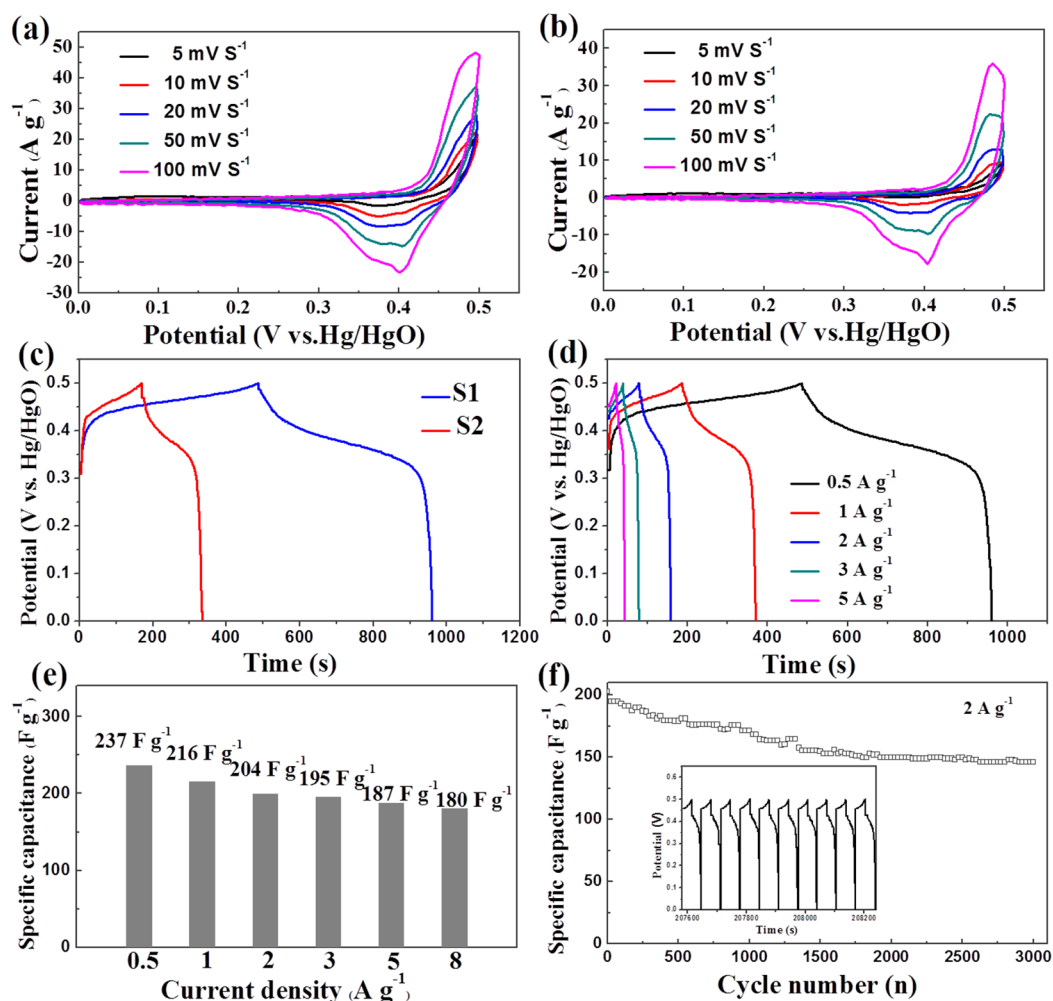
Figure 5. (a and b) CV curves of S-1 and S-2 at various scan rates. (c) Galvanostatic charge−discharge curves of S-1 and S-2 at a current density of 0.5 A g^{-1}. (d) Galvanostatic charge and discharge curves of S-1 at different current densities. (e) Rate performances of S-1 at various current densities. (f) Cycling performances of S-1 at a current density of 2 A g^{-1}; the inset in (f) shows the charge−discharge voltage profiles for the last 10 cycles at the same current density.

reactions. Therefore, it can be predicted that 3D hierarchical CuS microspheres (S-1) might show better performance in energy storage applications.

To qualitatively show the superiority of CuS microspheres (S-1) over thick nanoplates (S-2), we investigated the electrochemical behavior of two materials. Figure 5a,b depicts the CV curves of the S-1 and S-2 electrodes at different scan rates ranging from 5 to 100 mV s^{-1}. All the CV curves display a similar shape, which is different from an ideal rectangular shape, indicating pseudocapacitive characteristics. Obviously, a pair of redox peaks at can be observed 0.4 and 0.48 V; the redox reactions may be involved in the reaction between CuS and CuSOH,[40] which is similar to the redox reactions of CoS/CoSOH[41] and Ni(OH)$_2$/NiOOH[42] electrode, since Co, Ni, and Cu are in a contiguity family and show similar characteristics. The integrated areas of the S-1 electrode are substantially larger than those for the S-2 electrode at the same sweep rates in Figure 5a,b, suggesting that the specific capacitances of CuS microsphere supercapacitors are much larger than those for CuS platelike structure based devices.

Figure 5c shows charge−discharge (CD) curves for S-1 and S-2 electrodes obtained in a potential range between 0 and 0.5 V at a charging−discharging current density of 0.5 A g^{-1}. The

shapes of the CD curves indicate the characteristics of pseudocapacitance; the specific capacitance of S-1 (237 F g^{-1}) is calculated to be higher than that of S-2 (96 F g^{-1}), which is in agreement with the result of the CV measurements. In addition, CD curves of S-1 sample at current densities from 0.5 to 8 A g^{-1} are shown in Figure 5d. All the rapid CD curves show good electrochemical reversibility of the S-1 electrode within a stable potential window of 0−0.5 V. According to eq 1, Figure 5e calculates a series of specific capacitances against different current densities from the CD curves. The specific capacitances of CuS microspheres are 237, 216, 204, 195, 187, and 180 F g^{-1} at current densities of 0.5, 1, 2, 3, 5, and 8 A g^{-1}, respectively. About 75.9% of the original value is retained when the current density increases from 0.5 to 8 A g^{-1}. The result suggests a good rate capability.

The aforementioned results demonstrate that CuS microspheres show superior performance, which could be ascribed to the thin nanosheets and 3D hierarchical structure. Compared with the thick platelike structure, the thin nanosheets significantly shorten the diffusion pathway perpendicular to the facet and provide higher surface area, which increases the number of electrochemically active sites for the redox reaction.[43] Furthermore, the cavities among the nanosheets
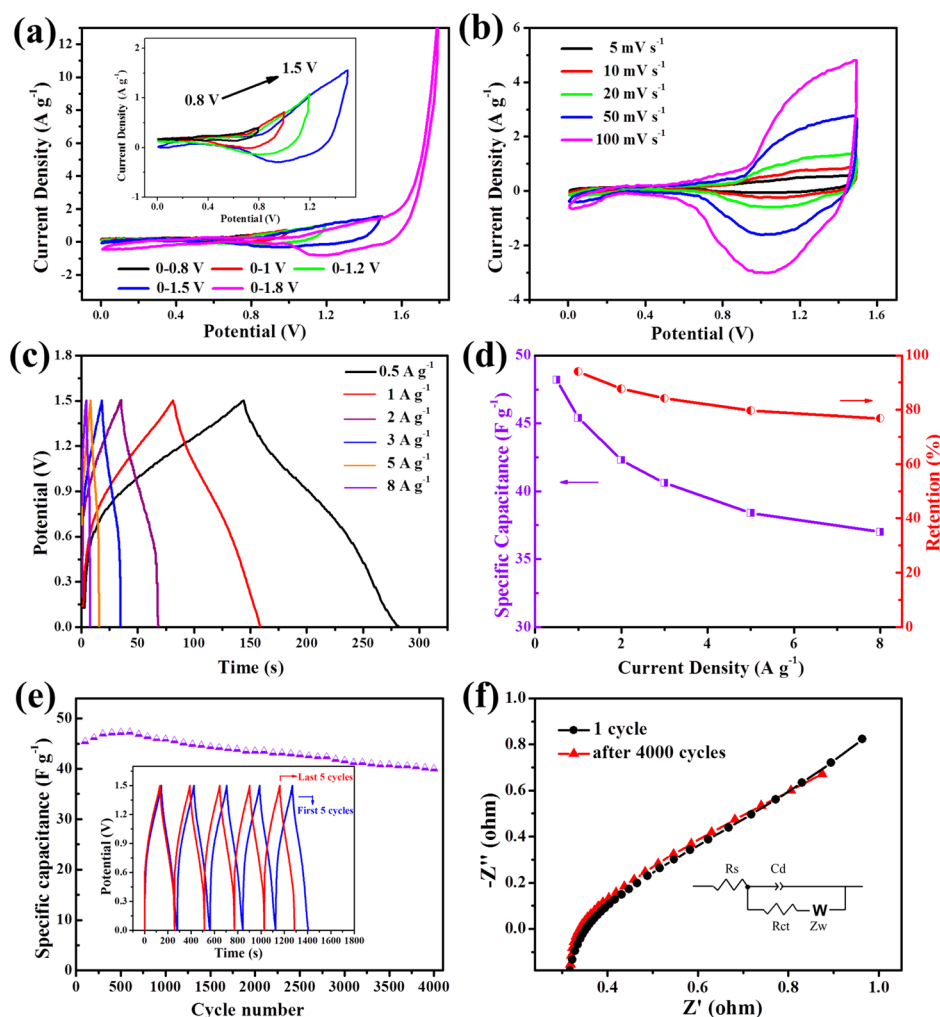
Figure 6. Electrochemical performance of a CuS//AC asymmetric supercapacitor. (a) CV curves of the CuS//AC asymmetric supercapacitor at different potential windows at 20 mV s^{-1}. (b) CV curves at different scan rates. (c) CD curves at different current densities. (d) Rate capability of the asymmetric supercapacitor. (e) Long-term cycling stability of the CuS//AC asymmetric supercapacitor at a current density of 1 A g^{-1}. (f) Nyquist plots of the first and 5000th cycles for the asymmetric supercapacitor at open current circuit; the inset is the expanded view.

can provide a larger pore volume, which is beneficial for sufficient contact between the electrolyte and electrode. Importantly, the enhanced accessible surface between the thin nanosheets can improve the electronic conductivity, and thus reduce the charge transfer resistance, which could be determined by the electrochemical impedance spectrum (EIS). As shown in Figure S9, the Nyquist plots of S-1 and S-2 electrodes indicate a low charge transfer resistance of the S-1 sample because of the negligible semicircle at a high frequency region. In a low frequency region, a greater slope of S-1 line compared to S-2 reveals a more facile ion diffusion to the surface of S-1 in the electrolyte and a more ideal capacitor behavior.[44]

Cycling performance is an important factor for evaluating a supercapacitor. The cycling stability of the S-1 electrode over 3000 cycles at a current density of 2 A g^{-1} is evaluated. As shown in Figure 5f, the 3D hierarchical nanostructured electrode shows good electrochemical stability and the specific capacitance loses only 26% after 3000 cycles. The inset of Figure 5f is the discharge–charge voltage profiles for the last 10 cycles of the CuS microspheres, which reveal a highly reversible charge–discharge process and good cycling performance. The 3D hierarchical structures play a key role for the stable cycling,

which can enhance the structural stability and flexibility, and prevent the nanosheets stacking on each other. The CuS samples obtained by [Bmim]$_2$CuCl$_4$ and [Omim]$_2$Cu$_2$Cl$_6$ have similar 3D hierarchical structures. We summarize the BET analysis and electrochemical performance of CuS samples synthesized by different precursors in Table S2. It is found that the BET specific surface areas of two CuS samples are larger than that of CuS nanoplates and the electrochemical performances of two samples are much better than that of CuS nanoplates, which further indicate the important role of 3D hierarchical structures. The specific capacitance and cycling stability of CuS electrode in our work reach a relatively high level compared with various CuS morphologies (Table S3), which further indicates the good electrochemical performance of CuS microspheres. Although some works (refs S4 and S5 in Supporting Information) report simple approaches without any surfactant or template to prepare different CuS structures with high specific capacitance, the temperature in their experiment is too high (150 °C), and the as-prepared samples are not uniform, which limits their cycling stability.

To further investigate the CuS electrode for real applications, an asymmetric supercapacitor device is fabricated by using AC as the negative electrodes and 3D hierarchical CuS micro-

spheres as the positive electrodes, respectively. CV curves of CuS and AC electrodes at a scan rate of 20 mV s^{-1} (Figure S10, Supporting Information) reveal that the CuS and AC electrodes have stable voltage windows of 0−0.5 V and −1 to 0 V, respectively. It could be expected that the voltage window could be extended to 1.5 V by the CuS//AC asymmetric super-capacitor. Figure 6a shows a series of CV curves collected at 20 mV s^{-1} with an operating ASC voltage ranging from 0.8 to 1.8 V to get the best operating potential of CuS//AC-ASC. As expected, the stable potential window without noticeable polarization curves can be obtained when the operational voltage of ASC is extended to as large as 1.5 V, which is larger than that of conventional AC-based symmetric supercapacitors (0.8−1.0 V) in aqueous electrolytes.[45] However, when the operational voltage reaches 1.8 V, oxygen will emerge. The typical CV curves of the CuS//AC-ASC device at different scan rates ranging from 5 to 100 mV s^{-1} are shown in Figure 6b. The increasing scan rate cannot obviously influence the shape of CV curves, indicating excellent reversibility and good rate capability of CuS//AC-ASC. Figure 6c demonstrates a galvanostatic charging−discharging measurement of CuS//AC-ASC at different current densities from 0.5 to 8 A g^{-1} with a potential window of 0−1.5 V. The slight nonlinearity of the discharge curves is attributed to the result of the redox reaction. Furthermore, the calculated specific capacitance values displayed in Figure 6d are 48.2, 45.4, 42.3, 40.6, 38.4, and 37 F g^{-1} at 0.5, 1, 2, 3, 5, and 8 A g^{-1}, respectively. It is noteworthy that CuS//AC-ASC could maintain 76.7% of capacitance retention even when the current density reaches 8 A g^{-1}, suggesting superior rate capability. Figure 6e presents the cycling stability of CuS//AC-ASC tested by carrying out continuous CD measurements over a current density of 1 A g^{-1} within the voltage window of 0−1.5 V. Obviously, the specific capacitance can still retain as high as 88% after 4000 cycles, which indicates the high cycle stability of the as-fabricated CuS//AC-ASC device. EIS measurement is employed to examine the change of charge transfer resistance before and after 4000 cycles. Figure 6f shows that CuS//AC-ASC exhibits no obvious resistance change after 4000 cycles compared to the first cycle, which further illustrates the excellent stability of the ASC device.

The energy and power density are important parameters to evaluate the performance of the asymmetric supercapacitor. Figure 7a shows the Ragone plot of the CuS//AC asymmetric supercapacitor device based on the CD measurement. A maximum energy density of 15.06 W h kg^{-1} can be obtained at a power density of 392.9 W kg^{-1}, and it still maintains 12 W h kg^{-1} even at a high power density of 4320 W kg^{-1}, which is advantageous over many symmetrical supercapacitors such as CNTs//CNTs (<10 W h kg^{-1}),[46] AC//AC supercapacitors (8 W h kg^{-1} at a power density of 35 kW kg^{-1}),[47] and 3D graphene/MnO$_2$//3D graphene/MnO$_2$ supercapacitors (6.8 W h kg^{-1} at a power density of 62 W kg^{-1}).[48] It is also higher than that of previously reported asymmetric supercapacitors such as Co(OH)$_2$-nanowires//AC-ASC (13.6 W h kg^{-1} at the power density of 153 W kg^{-1}),[49] Ni−Co/graphene//AC-ASC (7.6 W h kg^{-1} at the power density of 5600 W kg^{-1}),[50] Bi$_2$O$_3$//MnO$_2$-ASC (11.3 W h kg^{-1} at a power density of 352.6 W kg^{-1}),[51] and V$_2$O$_5$//RGO-ASC (13.3 W h kg^{-1} at a power density of 12.5 W kg^{-1}).[52] In practical applications, our asymmetric super-capacitors demonstrate the ability to power a commercial light-emitting diode (LED) well, although the capacitance grade is very low (Figure 7b).
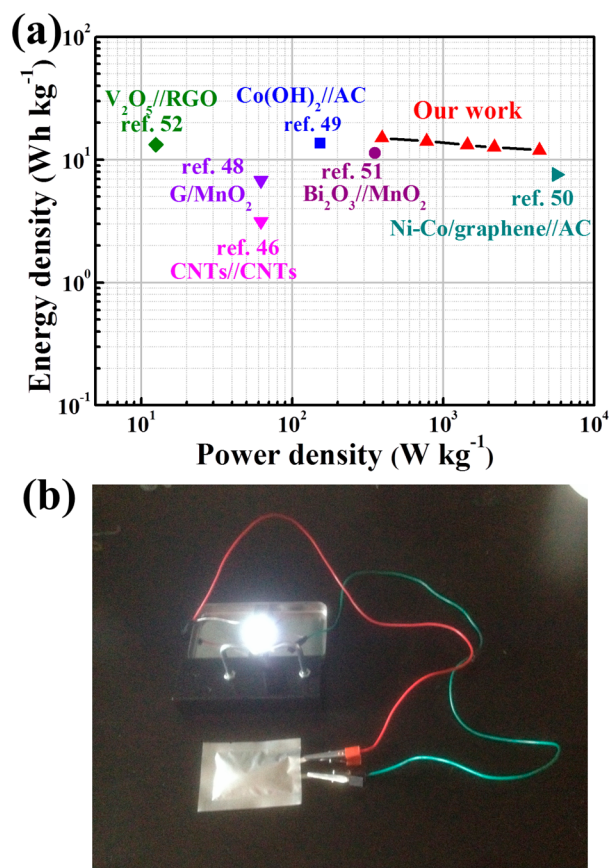
Figure 7. (a) Ragone plot of the CuS//AC asymmetric supercapacitor compared with other reported data. (b) Simple application to light a commercial light-emitting diode (LED).

■ CONCLUSIONS

In conclusion, 3D hierarchical CuS microspheres have been successfully prepared by a Cu-based IL precursor. During the fabrication of CuS, IL had directed the final structure, which includes the following: (1) the adsorption of alkyl imidazolium rings ([Bmim]$^+$) onto the (001) facets of covellite CuS inhibits the crystal growth along the [001] direction; (2) the alkyl chain had an influence on the assembly of CuS microspheres. The intriguing structural design (such as mesoporous structure, thin nanosheets subunit, and 3D well-defined hierarchical aggregate) and large specific surface area greatly enhance the electro-chemical performance for supercapacitors compared to tradi-tional synthesis materials, showing high specific capacitance (237 F g^{-1} at 0.5 A g^{-1}), good rate capability (retain 75.9% at 8 A g^{-1}), and stable cycle life (74% capacitance retention after 3000 cycles). An asymmetric supercapacitor (ASC) assembled by CuS and AC demonstrates an extended cycling performance with a large voltage window of 1.5 V (retains about 12% even after 4000 cycles) and exhibits an energy density of 15.06 W h kg^{-1} at a power density of 392.9 W kg^{-1}. The products are expected to be applied to other fields, such as solar cell devices, Li ion batteries, and photocatalysis, owing to their simple operation, low toxicity, and low cost.

■ ASSOCIATED CONTENT

S Supporting Information

The Supporting Information is available free of charge on the ACS Publications website at DOI: 10.1021/acsami.5b04452.

Structural view of $[Bmim]_2Cu_2Cl_6$; EDS spectrum of the obtained products; EDS spectrum, typical XPS spectra, and atomic ratio of CuS products obtained in 14 h; schematic illustration of crystal structure of $Cu(Tu)_3Cl$ and CuS; color transformation of different reaction times; SEM images and XRD patterns of CuS nanostructures obtained by $CuCl_2 \cdot 2H_2O$ and $[Bmim]_2CuCl_4$; SEM image of CuS nanostructure obtained by $[Omim]_2Cu_2Cl_6$; impedance Nyquist plots of S1 and S2 at open circuit potential; BET specific surface areas and electrochemical performance of CuS samples obtained by different precursors; electrochemical performance of as-prepared CuS microspheres compared with other CuS materials; comparative CV curves of 3D hierarchical CuS microspheres and AC electrodes at a scan rate of 20 mV s^{-1} in a three-electrode system (PDF)

■ AUTHOR INFORMATION

Corresponding Author
*E-mail: zhwj@nankai.edu.cn. Tel.: +86 22 23507951. Fax: +86 22 23502458.

Notes
The authors declare no competing financial interest.

■ ACKNOWLEDGMENTS

■ REFERENCES

(1) Whitesides, G. M.; Grzybowski, B. Self-assembly at All Scales. *Science* **2002**, *295*, 2418−2421.

(2) Zhang, Q. F.; Uchaker, E.; Candelaria, S. L.; Cao, G. Z. Nanomaterials for Energy Conversion and Storage. *Chem. Soc. Rev.* **2013**, *42*, 3127−3171.

(3) Ma, J. M.; Lei, D. N.; Duan, X. C.; Li, Q. H.; Wang, T. H.; Cao, A. M.; Mao, Y. H.; Zheng, W. J. Designable Fabrication of Flower-like SnS$_2$ Aggregates with Excellent Performance in Lithium-ion Batteries. *RSC Adv.* **2012**, *2*, 3615−3617.

(4) Wadia, C.; Alivisatos, A. P.; Kammen, D. M. Materials Availability Expands the Opportunity for Large-Scale Photovoltaics Deployment. *Environ. Sci. Technol.* **2009**, *43*, 2072−2077.

(5) Zhou, M.; Zhang, R.; Huang, M.; Lu, W.; Song, S. L.; Melancon, M. P.; Tian, M.; Liang, D.; Li, C. A Chelator-Free Multifunctional [^{64}Cu] CuS Nanoparticle Platform for Simultaneous Micro-PET/CT Imaging and Photothermal Ablation Therapy. *J. Am. Chem. Soc.* **2010**, *132*, 15351−15358.

(6) Zhang, J.; Yu, J.; Zhang, Y.; Li, Q.; Gong, J. R. Visible Light Photocatalytic H$_2$-Production Activity of CuS/ZnS Porous Nanosheets Based on Photoinduced Interfacial Charge Transfer. *Nano Lett.* **2011**, *11*, 4774−4779.

(7) Miller, T. A.; Wittenberg, J. S.; Wen, H.; Connor, S.; Cui, Y.; Lindenberg, A. M. The Mechanism of Ultrafast Structural Switching in Superionic Copper (I) Sulphide Nanocrystals. *Nat. Commun.* **2013**, *4*, 1369.

(8) Zhu, T.; Xia, B. Y.; Zhou, L.; Lou, X. W. Arrays of Ultrafine CuS Nanoneedles Supported on a CNT Backbone for Application in Supercapacitors. *J. Mater. Chem.* **2012**, *22*, 7851−7855.

(9) Peng, H.; Ma, G.; Sun, K.; Mu, J.; Wang, H.; Lei, Z. High-Performance Supercapacitor Based on Multi-Structural CuS@polypyrrole Composites Prepared by In Situ Oxidative Polymerization. *J. Mater. Chem. A* **2014**, *2*, 3303−3307.

(10) Chen, Y.; Davoisne, C.; Tarascon, J.; Guery, C. Growth of Single-Crystal Copper Sulfide Thin Films via Electrodeposition in Ionic Liquid Media for Lithium Ion Batteries. *J. Mater. Chem.* **2012**, *22*, 5295−5299.

(11) Mi, L.; Wei, W.; Zheng, Z.; Gao, Y.; Liu, Y.; Chen, W.; Guan, X. Tunable Properties Induced by Ion Exchange in Multilayer Intertwined CuS Microflowers with Hierarchal Structures. *Nanoscale* **2013**, *5*, 6589−6598.

(12) Cheng, Z.; Wang, S.; Wang, Q.; Geng, B. A Facile Solution Chemical Route to Self-Assembly of CuS Ball-flowers and Their Application as an Efficient Photocatalyst. *CrystEngComm* **2010**, *12*, 144−149.

(13) Bu, X.; Zhou, D.; Li, J.; Zhang, X.; Zhang, K.; Zhang, H.; Yang, B. Copper Sulfide Self-Assembly Architectures with Improved Photothermal Performance. *Langmuir* **2014**, *30*, 1416−1423.

(14) He, W.; Jia, H.; Li, X.; Lei, Y.; Li, J.; Zhao, H.; Mi, L.; Zhang, L.; Zheng, Z. Understanding the Formation of CuS Concave Superstructures with Peroxidase-Like Activity. *Nanoscale* **2012**, *4*, 3501−3506.

(15) Kundu, J.; Pradhan, D. Controlled Synthesis and Catalytic Activity of Copper Sulfide Nanostructured Assemblies with Different Morphologies. *ACS Appl. Mater. Interfaces* **2014**, *6*, 1823−1834.

(16) He, S.; Wang, G.; Lu, C.; Liu, J.; Wen, B.; Liu, H.; Guo, L.; Cao, M. Enhanced Wave Absorption of Nanocomposites Based on the Synthesized Complex Symmetrical CuS Nanostructure and Poly-(vinylidene fluoride). *J. Mater. Chem. A* **2013**, *1*, 4685−4692.

(17) Basu, M.; Sinha, A. K.; Pradhan, M.; Sarkar, S.; Negishi, Y.; Pal, T. Evolution of Hierarchical Hexagonal Stacked Plates of CuS from Liquid-Liquid Interface and Its Photocatalytic Application for Oxidative Degradation of Different Dyes under Indoor Lighting. *Environ. Sci. Technol.* **2010**, *44*, 6313−6318.

(18) Ma, J. M.; Mei, L.; Chen, Y. J.; Li, Q. H.; Wang, T. H.; Xu, Z.; Duan, X. C.; Zheng, W. J. α-Fe$_2$O$_3$ Nanochains: Ammonium Acetate-Based Ionothermal Synthesis and Ultrasensitive Sensors for Low-ppm-level H$_2$S Gas. *Nanoscale* **2013**, *5*, 895−898.

(19) Greaves, T. L.; Drummond, C. J. Solvent Nanostructure, the Solvophobic Effect and Amphiphile Self-Assembly in Ionic Liquids. *Chem. Soc. Rev.* **2013**, *42*, 1096−1120.

(20) Taubert, A. CuCl Nanoplatelets from an Ionic Liquid-Crystal Precursor. *Angew. Chem., Int. Ed.* **2004**, *43*, 5380−5382.

(21) Duan, X.; Ma, J.; Lian, J.; Zheng, W. The Art of Using Ionic Liquids in the Synthesis of Inorganic Nanomaterials. *CrystEngComm* **2014**, *16*, 2550−2559.

(22) Xia, J.; Yin, S.; Li, H.; Xu, H.; Yan, Y.; Zhang, Q. Self-Assembly and Enhanced Photocatalytic Properties of BiOI Hollow Microspheres via a Reactable Ionic Liquid. *Langmuir* **2011**, *27*, 1200−1206.

(23) Duan, X.; Li, D.; Zhang, H.; Ma, J.; Zheng, W. Crystal-Facet Engineering of Ferric Giniite by Using Ionic-Liquid Precursors and Their Enhanced Photocatalytic Performances under Visible-Light Irradiation. *Chem. - Eur. J.* **2013**, *19*, 7231−7242.

(24) Xu, H.; Li, H. M.; Xia, J. X.; Yin, S.; Luo, Z. J.; Liu, L.; Xu, L. One-Pot Synthesis of Visible-Light-Driven Plasmonic Photocatalyst Ag/AgCl in Ionic Liquid. *ACS Appl. Mater. Interfaces* **2011**, *3*, 22−29.

(25) Liu, X.; Duan, X.; Peng, P.; Zheng, W. Hydrothermal Synthesis of Copper Selenides with Controllable Phases and Morphologies from an Ionic Liquid Precursor. *Nanoscale* **2011**, *3*, 5090−5095.

(26) Li, C.; Gu, L.; Tsukimoto, S.; van Aken, P. A.; Maier, J. Low-Temperature Ionic-Liquid-Based Synthesis of Nanostructured Iron-Based Fluoride Cathodes for Lithium Batteries. *Adv. Mater.* **2010**, *22*, 3650−3654.

(27) Xu, L.; Xia, J.; Wang, L.; Qian, J.; Li, H.; Wang, K.; Sun, K.; He, M. α-Fe$_2$O$_3$ Cubes with High Visible-Light-Activated Photoelectrochemical Activity towards Glucose: Hydrothermal Synthesis Assisted by a Hydrophobic Ionic Liquid. *Chem. - Eur. J.* **2014**, *20*, 2244−2253.

(28) Ge, L.; Jing, X.; Wang, J.; Jamil, S.; Liu, Q.; Song, D.; Wang, J.; Xie, Y.; Yang, P.; Zhang, M. Ionic Liquid-Assisted Synthesis of CuS Nest Like Hollow Spheres Assembled by Microflakes Using an Oil Water Interface Route. *Cryst. Growth Des.* **2010**, *10*, 1688−1692.

(29) Yao, K.; Lu, W.; Li, X.; Wang, J. Ionic Liquids-Modulated Two-Phase Thermal Synthesis of Three-Dimensional CuS Nanostructures. *J. Solid State Chem.* **2012**, *196*, 557−564.

(30) Wu, C. Y.; Yu, S. H.; Antonietti, M. Complex Concaved Cuboctahedrons of Copper Sulfide Crystals with Highly Geometrical Symmetry Created by a Solution Process. *Chem. Mater.* **2006**, *18*, 3599−3601.

(31) Zhu, T.; Nuo Peh, C. K.; Hong, M. H.; Ho, G. W. Outside-In Recrystallization of ZnS−Cu₁.₈S Hollow Spheres with Interdispersed Lattices for Enhanced Visible Light Solar Hydrogen Generation. *Chem. - Eur. J.* **2014**, *20*, 11505−11510.

(32) Okaya, Y.; Knobler, C. B. Refinement of the Crystal Structure of Tris (thiourea) Copper(I) Chloride. *Acta Crystallogr.* **1964**, *17*, 928−930.

(33) Bombicz, P.; Mutikainen, I.; Krunks, M.; Leskela, T.; Madarasz, J.; Niinisto, L. Synthesis, Vibrational Spectra and X-ray Structures of Copper(I) Thiourea Complexes. *Inorg. Chim. Acta* **2004**, *357*, 513−525.

(34) Dean, J. A. *Lange's Handbook of Chemistry*, 11th ed.; McGraw-Hill Professional Publishing: New York, 1973; p 5-45-65.

(35) Lu, W.; Ding, Y.; Chen, Y.; Wang, Z. L.; Fang, J. Bismuth Telluride Hexagonal Nanoplatelets and Their Two-Step Epitaxial Growth. *J. Am. Chem. Soc.* **2005**, *127*, 10112−10116.

(36) Jin, J.; Iyoda, T.; Cao, C.; Song, Y.; Jiang, L.; Li, T. J.; Zhu, D. B. Self-Assembly of Uniform Spherical Aggregates of Magnetic Nanoparticles Through pi-pi Interactions. *Angew. Chem., Int. Ed.* **2001**, *40*, 2135−2138.

(37) Qi, K. Z.; Qin, Q.; Duan, X. C.; Wang, G. C.; Wu, L. Y.; Zheng, W. J. Geometric Matching Principle for Adsorption Selectivity of Ionic Liquids: A Simple Method into the Fascinating World of Shape-Controlled Chemistry. *Chem. - Eur. J.* **2014**, *20*, 9012−9017.

(38) Zheng, W. J.; Liu, X. D.; Yan, Z. Y.; Zhu, L. J. Ionic Liquid-Assisted Synthesis of Large-Scale TiO₂ Nanoparticles with Controllable Phase by Hydrolysis of TiCl₄. *ACS Nano* **2009**, *3*, 115−122.

(39) Bowlas, C. J.; Bruce, D. W.; Seddon, K. R. Liquid-Crystalline Ionic Liquids. *Chem. Commun.* **1996**, *14*, 1625−1626.

(40) Qian, L.; Tian, X.; Yang, L.; Mao, J.; Yuan, H.; Xiao, D. High Specific Capacitance of CuS Nanotubes in Redox Active Polysulfide Electrolyte. *RSC Adv.* **2013**, *3*, 1703−1708.

(41) Tao, F.; Zhao, Y. Q.; Zhang, G. Q.; Li, H. L. Electrochemical Characterization on Cobalt Sulfide for Electrochemical Supercapacitors. *Electrochem. Commun.* **2007**, *9*, 1282−1287.

(42) Yang, J.; Duan, X.; Qin, Q.; Zheng, W. Solvothermal Synthesis of Hierarchical Flower-like β-NiS with Excellent Electrochemical Performance for Supercapacitors. *J. Mater. Chem. A* **2013**, *1*, 7880−7884.

(43) Chhowalla, M.; Shin, H. S.; Eda, G.; Li, L.-J.; Loh, K. P.; Zhang, H. The Chemistry of Two-Dimensional Layered Transition Metal Dichalcogenide Nanosheets. *Nat. Chem.* **2013**, *5*, 263−275.

(44) Yang, J. Q.; Duan, X. C.; Guo, W.; Li, D.; Zhang, H. L.; Zheng, W. J. Electrochemical Performances Investigation of NiS/rGO Composite as Electrode Material for Supercapacitors. *Nano Energy* **2014**, *5*, 74−81.

(45) Moosavifard, S. E.; El-Kady, M. F.; Rahmanifar, M. S.; Kaner, R. B.; Mousavi, M. F. Designing 3D Highly Ordered Nanoporous CuO Electrodes for High-Performance Asymmetric Supercapacitors. *ACS Appl. Mater. Interfaces* **2015**, *7*, 4851−4860.

(46) Yu, C.; Masarapu, C.; Rong, J.; Wei, B.; Jiang, H. Stretchable Supercapacitors Based on Buckled Single-Walled Carbon-Nanotube Macrofilms. *Adv. Mater.* **2009**, *21*, 4793−4797.

(47) Qu, Q.; Zhu, Y.; Gao, X.; Wu, Y. Core−Shell Structure of Polypyrrole Grown on V₂O₅ Nanoribbon as High Performance Anode Material for Supercapacitors. *Adv. Energy Mater.* **2012**, *2*, 950−955.

(48) He, Y.; Chen, W.; Li, X.; Zhang, Z.; Fu, J.; Zhao, C.; Xie, E. Freestanding Three-Dimensional Graphene/MnO₂ Composite Networks as Ultralight and Flexible Supercapacitor Electrodes. *ACS Nano* **2013**, *7*, 174−182.

(49) Tang, Y.; Liu, Y.; Yu, S.; Mu, S.; Xiao, S.; Zhao, Y.; Gao, F. Morphology Controlled Synthesis of Monodisperse Cobalt Hydroxide for Supercapacitor with High Performance and Long Cycle Life. *J. Power Sources* **2014**, *256*, 160−169.

(50) Wang, H. L.; Holt, C. M. B.; Li, Z.; Tan, X. H.; Amirkhiz, B. S.; Xu, Z. W.; Olsen, B. C.; Stephenson, T.; Mitlin, D. Graphene-Nickel Cobaltite Nanocomposite Asymmetrical Supercapacitor with Commercial Level Mass Loading. *Nano Res.* **2012**, *5*, 605−617.

(51) Xu, H. H.; Hu, X. L.; Yang, H. L.; Sun, Y. M.; Hu, C. C.; Huang, Y. H. Flexible Asymmetric Micro-Supercapacitors Based on Bi₂O₃ and MnO₂ Nanoflowers: Larger Areal Mass Promises Higher Energy Density. *Adv. Energy Mater.* **2015**, DOI: 10.1002/aenm.201401882.

(52) Foo, C. Y.; Sumboja, A.; Tan, D. J. H.; Wang, J. X.; Lee, P. S. Flexible and Highly Scalable V₂O₅-rGO Electrodes in an Organic Electrolyte for Supercapacitor Devices. *Adv. Energy Mater.* **2014**, DOI: 10.1002/aenm.201400236.